Communication: State-to-state photodissociation study by the two-color VUV-VUV laser pump-probe time-slice velocity-map-imaging-photoion method

Hong Gao, Yu Song, William M. Jackson, and C. Y. Ng

Citation: J. Chem. Phys. **138**, 191102 (2013); doi: 10.1063/1.4807302
View online: http://dx.doi.org/10.1063/1.4807302
View Table of Contents: http://jcp.aip.org/resource/1/JCPSA6/v138/i19
Published by the American Institute of Physics.

Communication: State-to-state photodissociation study by the two-color VUV-VUV laser pump-probe time-slice velocity-map-imaging-photoion method

Hong Gao, Yu Song, William M. Jackson,[a] and C. Y. Ng[a]
Department of Chemistry, University of California, Davis, California 95616, USA

(Received 21 March 2013; accepted 3 May 2013; published online 16 May 2013)

We demonstrate that combining two independently tunable vacuum ultraviolet (VUV) lasers and the time-slice velocity-map-imaging-photoion (VMI-PI) method allows the rovibronically state-selected photodissociation study of CO in the VUV region along with the state-selective detection of product $C(^3P_{0,1,2})$ using the VUV-UV $(1+1')$ resonance-enhanced photoionization and the VUV Rydberg autoionization methods. Both tunable VUV lasers are generated based on the two-photon resonance-enhanced four-wave mixing scheme using a pulsed rare gas jet as the nonlinear medium. The observed fine-structure distributions of product $C(^3P_J)$, J = 0, 1, and 2, are found to depend on the CO rovibronic state populated by VUV photoexcitation. The branching ratios for $C(^3P_0) + O(^3P_J)$: $C(^3P_0) + O(^1D_2)$, $C(^3P_1) + O(^3P_J)$: $C(^3P_1) + O(^1D_2)$, and $C(^3P_2) + O(^3P_J)$: $C(^3P_2) + O(^1D_2)$, which were determined based on the time-slice VMI-PI measurements of C^+ ions formed by J-state selective photoionization sampling of $C(^3P_{0,1,2})$, also reveal strong dependences on the spin-orbit state of $C(^3P_{0,1,2})$. By combining the measured branching ratios and fine-structure distributions of $C(^3P_{0,1,2})$, we have determined the correlated distributions of $C(^3P_{0,1,2})$ accompanying the formation of $O(^1D_2)$ and $O(^3P_J)$ produced in the VUV photodissociation of CO. The success of this demonstration experiment shows that the VUV photodissociation pump-VUV photoionization probe method is promising for state-to-state photodissociation studies of many small molecules, which are relevant to planetary atmospheres as well as fundamental understanding of photodissociation dynamics. © *2013 AIP Publishing LLC*. [http://dx.doi.org/10.1063/1.4807302]

Dissociation is generally the major decay pathway for molecular species following vacuum ultraviolet (VUV) photoexcitation (PEX) to energy levels above the dissociation thresholds. The ultimate goal for understanding VUV photodissociation dynamics is to achieve control of selective bond breaking processes in molecular dissociation via photoexcitation. In addition to gaining fundamental understanding, many previous photodissociation studies were motivated by their relevant applications to a variety of research fields, such as astrophysics and planetary chemistry. There are many known experimental schemes for the study of photodissociation dynamics.[1] In the energy domain, state-to-state measurements, which involve the determination of quantum state and angular distributions of photofragments produced from the unimolecular decomposition of state- or energy-selected parent species, remain the most direct and informative scheme for the study of photodissociation dynamics.

We have recently developed a VUV laser velocity-map-imaging-photoion (VMI-PI) apparatus for state-to-state VUV photodissociation studies of CO, N_2, and NO.[2–7] This apparatus consists of a broadly tunable VUV laser source for photoexcitation of molecules to selected predissociative states and a time-slice VMI-PI detection system for total kinetic energy release (TKER) measurements. The VUV laser is generated by the two-photon resonance-enhanced four-wave frequency mixing (TP-RE-FWFM) scheme using a rare gas jet as the nonlinear medium. In these VUV experiments, we found that the same VUV photolysis laser can also be used for the photoionization (PI) probe of photofragment states, allowing VMI-PI measurements to be performed. Nevertheless, we found that due to the lack of independent tunability of the VUV photoionization energy, the VUV laser VMI-PI apparatus does not allow the optimization of experimental conditions for state-selective photoionization detection. In this Communication, we report the successful development of the VUV-VUV laser VMI-PI apparatus by implementation of a second tunable VUV laser with the previously established VUV laser VMI-PI apparatus for state-to-state VUV photodissociation studies.

The resonance-enhanced multiphoton ionization (REMPI) scheme is a popular method for photoionization probes of nascent photofragment states. For REMPI detection, it is desirable for the photofragment to have a stable intermediate state, and to focus the photoionization laser at the interaction region. The small ionization volume resulting from focusing the laser can reduce the detection sensitivity, especially when the photolysis source is an unfocused VUV laser. The high ion yield produced in REMPI detection can also lower the achievable kinetic energy resolution in VMI-PI measurements due to the space-charge effect. Most of these disadvantages can be avoided by adopting a state-selective detection scheme involving VUV excitation of photofragments to a Rydberg state as a first step. For a Rydberg state

[a]Authors to whom correspondence should be addressed. Electronic addresses: wmjackson@ucdavis.edu and cyng@ucdavis.edu.

formed above the IE of the photofragment, prompt autoionization can readily occur. For a Rydberg state formed below the ionization energy (IE) of the photofragment, ionization of the excited photofragments can be efficiently accomplished by absorbing an additional visible (VIS) or UV photon. This VUV (1+1′) resonance-enhanced photoionization scheme was proposed previously by Kung and Lee.[8] Since the VUV Rydberg autoionization and the VUV (1+1′) photoionization schemes described above are mediated by a resonant Rydberg state, they have significantly higher efficiencies for photoionization samplings than that achieved by direct photoionization. Considering that the VUV laser radiation generated by the TP-RE-FWFM schemes is tunable in the range of ≈7–19 eV, which covers the IEs of nearly all atomic and molecular species, the VUV (1+1′) photoionization and VUV Rydberg autoionization schemes can be generally applicable for photodissociation studies of essentially all molecular systems. The VUV-VUV laser VMI-PI apparatus is developed with the application of these state-selective photoionization schemes in mind.

In this experiment, we have selected the state-to-state VUV photodissociation of CO as a demonstration study. Being the third most abundance species in the universe, the VUV photodissociation of CO plays an important role in astrophysics.[9] To our knowledge, the study of the photodissociation dynamics of CO to the state-to-state detail has not been made previously. We show that the ability to independently tune the energy of the VUV photoionization laser has enhanced the sensitivity of the experiment by more than two orders of magnitude compared to that observed by using a single VUV laser for both photodissociation excitation and photoionization sampling.[4] This improvement has made possible the unambiguous determination of the fine-structure distribution of product $C(^3P_{0,1,2})$. This together with the branching ratio measurements has allowed the determination of the correlated distributions of $C(^3P_{0,1,2})$ with other photoproducts $O(^1D_2)$ and $O(^3P_J)$ in the VUV photodissociation of CO.

Figure 1 depicts the schematic diagram of the newly developed VUV-VUV laser VMI-PI apparatus designed for state-to-state VUV photodissociation studies of gaseous molecules. This apparatus is modified from the VUV laser time-slice VMI-PI spectrometer reported previously[2–6] by adding a second independently tunable VUV laser. While the original VUV laser (VUV-I) was used as the photodissociation source, the added VUV laser (VUV-II) was employed for VUV state-selective photoionization probes. Both VUV-I and VUV-II have the same basic design [repetition rate = 30 Hz, VUV optical bandwidth = 0.4 cm^{-1} (FWHM)] and are generated by the TP-RE-FWFM schemes, providing tunable VUV sum-frequency ($2\omega_1 + \omega_2$) and different-frequency ($2\omega_1 - \omega_2$), where ω_1 and ω_2 represent the respective UV and VIS outputs of the dye lasers. By tuning ω_2 in the range of 400-900 nm with ω_1 fixed at appropriate $2\omega_1$ resonant transition frequencies of the nonlinear medium (Kr or Xe), the ($2\omega_1 - \omega_2$) and ($2\omega_1 + \omega_2$) frequencies can be readily generated in the ranges of 6.9–11.5 and 11.3–16.0 eV, respectively. The VUV-I and VUV-II beams enter the PI/PEX center head to head and perpendicular to the central axis of the VMI-PI apparatus. A movable LiF window is in the path of the VUV-II beam so that we can block or unblock the sum-frequency of the VUV-II beam as needed.

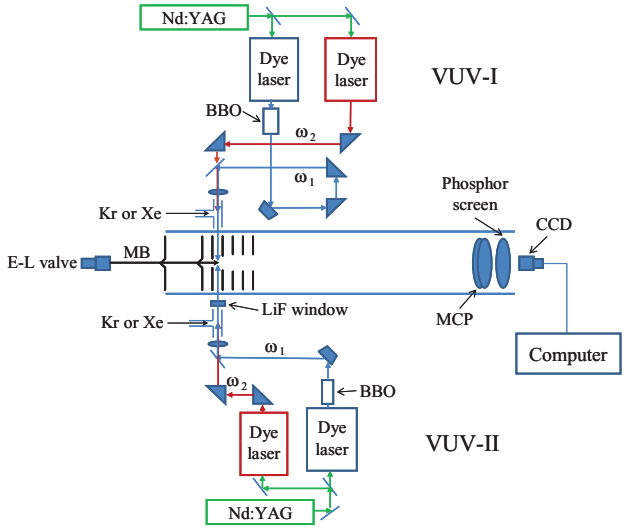

FIG. 1. Schematic diagram of the VUV-VUV laser VMI-PI apparatus.

The CO sample is introduced into the PI/PEX region in the form of a pulsed supersonic CO beam by using an Even-Lavie pulsed valve (nozzle diameter = 0.2 mm, CO stagnation pressure = 50 psi, repetition rate = 30 Hz) traveling along the central axis of the VMI-PI apparatus. The CO beam was skimmed by 2 conical skimmers prior to intersecting the VUV lasers at the PI/PEX center. The VUV photodissociation of CO was achieved by tuning VUV-I to the R(0) lines of the CO vibronic states $(4s\sigma)\,^1\Sigma^+(v=4)$, $(4p\sigma)\,^1\Sigma^+(v=3)$, and $(4p\pi)\,^1\Pi\,(v=3)$ at 109 452.6, 109 484.7, and 109 568.6 cm^{-1}, respectively.[10]

The measurement of the fine-structure distribution of product $C(^3P_{0,1,2})$ is based on the VUV (1+1′) photoionization method without using the VMI technique, in which $C(^3P_{0,1,2})$ atoms are first excited by VUV-II to the excited intermediate Rydberg state $C^*[2s^22p4s\ (^3P_{0,1,2})]$ or $C^*[2s^22p3d\ (^3D_{1,2,3})]$ lying below the IE(C). The ionization of these Rydberg states can be readily accomplished by absorbing a UV photon from the ω_1 laser beam, which is also a component of the VUV-II beam. During this measurement, the LiF window was inserted into the path of VUV-II to eliminate the photodissociation caused by the sum-frequency component of the VUV-II beam. By scanning the VUV-II laser in the region of 78 065–78 135 cm^{-1} (78 245–78 300 cm^{-1}) for excitation of $C(^3P_{0,1,2})$ to the $C^*[2s^22p4s\ (^3P_{0,1,2})]$ $\{C^*[2s^22p3d\ (^3D_{1,2,3})]\}$ state, we have obtained the VUV (1+1′) photoion spectra of $C(^3P_{0,1,2})$ produced by predissociation of the rovibronically selected states $(4s\sigma)\,^1\Sigma^+(v=4)$, $(4p\sigma)\,^1\Sigma^+(v=3)$, and $(4p\pi)\,^1\Pi(v=3)$ of CO as depicted in Figs. 2(a) and 2(d), 2(b) and 2(e), and 2(c) and 2(f), respectively. The peaks are broadened due to the Doppler effect caused by recoils of the photofragments. The intensities of the peaks at 78 073.2 cm^{-1} (78 264.0 cm^{-1}) observed in Figs. 2(a)–2(c) [2(d)–2(f)] were arbitrarily normalized to the same value. The assignment of the transitions between the spin-orbit states of $C(^3P_{0,1,2})$ and those of the intermediate Rydberg states are marked in the top spectra of Fig. 2.

TABLE I. Fine-structure populations (F0, F1, and F2) in % of C atoms in the respective C($^3P_0$, $^3P_1$, and $^3P_2$) states formed by VUV photodissociation of CO excited in the $N = 1$ rotational levels of the $(4s\sigma)^1\Sigma^+(v = 4)$, $(4p\sigma)^1\Sigma^+(v = 3)$, and $(4p\pi)^1\Pi(v = 3)$ states.[a,b]

	Common intermediate state: C*[$2s^2 2p4s$ ($^3P_1$)]			Common intermediate state: C*[$2s^2 2p3d$ ($^3D_1$)]		
Predissociative CO states	F0	F1	F2	F0	F1	F2
$(4s\sigma)^1\Sigma^+(v = 4)$	69 ± 2 (247 ± 5)	10 ± 2 (18 ± 3)	21 ± 2 (74 ± 5)	67 ± 4 (851 ± 11)	8 ± 3 (71 ± 5)	25 ± 3 (15 ± 2)
$(4p\sigma)^1\Sigma^+(v = 3)$	54 ± 2 (190 ± 6)	24 ± 2 (46 ± 4)	22 ± 2 (80 ± 5)	51 ± 4 (641 ± 8)	23 ± 3 (215 ± 4)	26 ± 2 (15 ± 1)
$(4p\pi)^1\Pi(v = 3)$	28 ± 4 (95 ± 5)	40 ± 4 (76 ± 5)	32 ± 5 (117 ± 14)	30 ± 9 (390 ± 110)	33 ± 12 (300 ± 130)	37 ± 2 (22 ± 5)

[a]Values determined by the VUV (1+1′) photoionization method. See the text.
[b]The values in parentheses are the relative intensities of the transition peaks (marked by red arrows) in the spectra of Figs. 2(a)–2(f).

We note that all three spin-orbit levels C($^3P_{0,1,2}$) can be excited to the common intermediate levels C*[$2s^2 2p4s$ ($^3P_1$)] and C*[$2s^2 2p3d$ ($^3D_1$)]. Since the VUV-II intensities in the energy ranges of Figs. 2(a)–2(e) are constant and the photoionization efficiencies of the three spin-orbit levels C($^3P_0$, $^3P_1$, and $^3P_2$) via the common intermediate level C*[$2s^2 2p4s$ ($^3P_1$)] {C*[$2s^2 2p3d$ ($^3D_1$)]} as measured by the relative intensities of the transition peaks [marked by red arrows in Figs. 2(a)–2(e)] should be governed by the corresponding transition probabilities of C*[$2s^2 2p4s$ ($^3P_1$)] ← C($^3P_0$, $^3P_1$, and $^3P_2$) {C*[$2s^2 2p3d$ ($^3D_1$)] ← C($^3P_0$, $^3P_1$, and $^3P_2$)} and the nascent fine-structure populations of C($^3P_0$, $^3P_1$, and $^3P_2$). The relative intensities of the transition peaks, which were determined by taking the areas under the peaks, are given in parentheses in Table I. After correcting for the transition probabilities of 3.55×10^7, 1.87×10^7, and 3.62×10^7 for the C*[$2s^2 2p4s$ ($^3P_1$)] ← C($^3P_0$, $^3P_1$, $^3P_2$) transitions, and 1.26×10^8, 9.24×10^7, and 5.94×10^6 for the C*[$2s^2 2p3d$ ($^3D_1$)] ← C($^3P_0$, $^3P_1$, $^3P_2$) transitions,[11] respectively, we have obtained the fine-structure populations (in %) F0, F1, and F2 for C($^3P_0$), C($^3P_1$), and C($^3P_2$), respectively, produced by VUV-I photodissociation of CO excited in the $N = 1$ rotational level of the $(4s\sigma)^1\Sigma^+(v = 4)$, $(4p\sigma)^1\Sigma^+(v = 3)$, and $(4p\pi)^1\Pi(v = 3)$ states as listed in Table I. The transition probabilities were obtained recently by accurate theoretical calculations.[11]

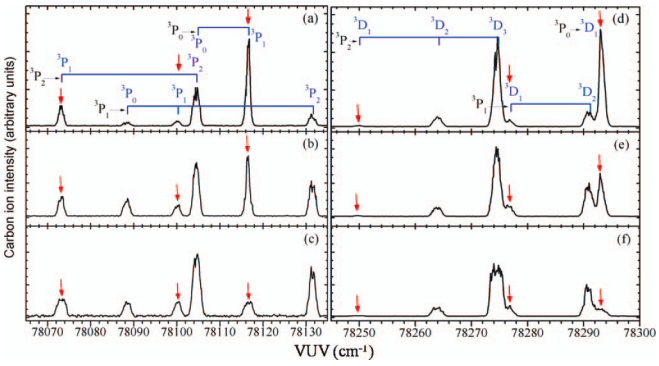

FIG. 2. VUV (1+1′) photoion spectra of C($^3P_{0,1,2}$) obtained via the intermediate states C*[$2s^2 2p4s$ ($^3P_{0,1,2}$)] and C*[$2s^2 2p3d$ ($^3D_{1,2,3}$)] are depicted in (a), (b), and (c) and (d), (e), and (f), respectively. The VUV-I frequencies are set at 109 452.6 cm^{-1} for (a) and (d), 109 484.7 cm^{-1} for (b) and (e), and 109 568.6 cm^{-1} for (c) and (f), which correspond to the respective excitation energies of the CO states $(4s\sigma)\ ^1\Sigma^+(v = 4)$, $(4p\sigma)\ ^1\Sigma^+\ (v = 3)$, and $(4p\pi)\ ^1\Pi\ (v = 3)$. The assignments of the peaks are shown by drop lines; and the terms of the ground and intermediate Rydberg states of C are shown in black and blue, respectively. The peaks are broadened due to the Doppler effect caused by the recoils of the photofragments.

As shown in the table, the spin-orbit distributions determined via the two intermediate states C*[$2s^2 2p4s$ ($^3P_1$)] and C*[$2s^2 2p3d$ ($^3D_1$)] are in good agreement within the experimental uncertainties. This observation confirms the validity of the VUV (1+1′) photoionization method for determining the fine-structure distribution of C($^3P_{0,1,2}$) and the reliability of the calculated transition probabilities. The fine-structure distributions thus determined are found to be strongly dependent on the rovibronic states of CO being excited.

Correlated internal state distributions of photofragments provide the most detailed information about the photodissociation dynamics.[12,13] However, such measurements have been highly challenging. Correlated spin-orbit branching ratios of O($^3P_{2,1,0}$) in the photodissociation of O_2 and OH, and Cl($^2P_{3/2,\ 1/2}$) in the photodissociation of ClO have been measured previously.[13–16] Compared with O($^3P_{2,1,0}$) and Cl($^2P_{3/2,\ 1/2}$), the spin-orbit splitting of C($^3P_{0,1,2}$) is significantly smaller, making it much more difficult to employ the methods used in the above experiments[13–16] for determining the correlated spin-orbit branching ratios of C($^3P_{0,1,2}$) with other photofragments.

We have successfully determined the correlated fine-structure distribution of C($^3P_{0,1,2}$) accompanying O($^1D_2$) and O(^3P_J) formed in the VUV-I photodissociation of CO using the VUV-VUV laser VMI-PI apparatus. Here, the first step involves the measurement of branching ratios I (BR-I), II (BR-II), and III (BR-III), as defined in Eqs. (1)–(3), respectively,

$$\text{BR-I} = [\text{C}(^3\text{P}_0) + \text{O}(^1\text{D}_2)]/\{[\text{C}(^3\text{P}_0) + \text{O}(^3\text{P}_J)] + [\text{C}(^3\text{P}_0) + \text{O}(^1\text{D}_2)]\}, \quad (1)$$

$$\text{BR-II} = [\text{C}(^3\text{P}_1) + \text{O}(^1\text{D}_2)]/\{[\text{C}(^3\text{P}_1) + \text{O}(^3\text{P}_J)] + [\text{C}(^3\text{P}_1) + \text{O}(^1\text{D}_2)]\}, \quad (2)$$

TABLE II. Branching ratios [BR-I, BR-II, and BR-III defined by Eqs. (1)–(3)] obtained using the VUV Rydberg autoionization and time-slice VMI-PI methods.

Predissociative CO states[a]	BR-I[b]	BR-II	BR-III
$(4s\sigma)^1\Sigma^+(v = 4)$	0.62 ± 0.03	0.09 ± 0.01	0.08 ± 0.01
$(4p\sigma)^1\Sigma^+(v = 3)$	0.37 ± 0.02	0.03 ± 0.02	0.12 ± 0.01
$(4p\pi)^1\Pi(v = 3)$	0.20 ± 0.01	0.59 ± 0.03	0.13 ± 0.01

[a]The $N = 1$ rotational levels of the predissociative states of CO are excited.
[b]The C($^1D_2$) + O(^3P_J) channel is not probed here; and thus is ignored in the analysis.

TABLE III. Correlated fine-structure distribution (in %) of $C(^3P_{0,1,2})$ accompanying with $O(^1D)$ and $O(^3P_J)$.[a]

Predissociative CO state	$C(^3P_2) + O(^1D_2)$	$C(^3P_1) + O(^1D_2)$	$C(^3P_0) + O(^1D_2)$	$C(^3P_2) + O(^3P_J)$	$C(^3P_1) + O(^3P_J)$	$C(^3P_0) + O(^3P_J)$
$(4s\sigma)^1\Sigma^+(v=4)$	1.7 ± 0.3	0.9 ± 0.2	42.4 ± 3.0	19.3 ± 2.0	9.1 ± 1.9	26.6 ± 2.3
$(4p\sigma)^1\Sigma^+(v=3)$	2.7 ± 0.4	0.7 ± 0.4	19.7 ± 1.6	19.3 ± 1.9	23.3 ± 2.3	34.3 ± 2.2
$(4p\pi)^1\Pi(v=3)$	4.3 ± 1.1	23.4 ± 3.4	5.5 ± 0.9	27.7 ± 4.8	16.6 ± 2.7	22.5 ± 3.3

[a]Since the $C(^1D_2) + O(^3P_J)$ channel is not measured in this study, the sum of the distributions of the six channels listed in the table can be set as 100%.

$$\text{BR-III} = [C(^3P_2) + O(^1D_2)]/\{[C(^3P_2) + O(^3P_J)] + [C(^3P_2) + O(^1D_2)]\}. \quad (3)$$

To selectively probe the spin-orbit states $C(^3P_0)$, $C(^3P_1)$, and $C(^3P_2)$ produced by VUV-I photodissociation of CO, VUV-II is tuned to the excitation transitions $C^*[2s2p^3\ (^3S_1)] \leftarrow C(^3P_0, {}^3P_1,$ and $^3P_2)$ at 105 799.3, 105 782.6, and 105 755.7 cm^{-1}, respectively. Since the excited $C^*[2s2p^3\ (^3S_1)]$ state is above the IE(C), it will undergo prompt autoionization. The resulting C^+ ions are analyzed by the time-slice VMI-PI method to provide the TKER spectra, in which two peaks corresponding to the formation of the dissociation channels $C(^3P_{0,1,2}) + O(^3P_J)$ and $C(^3P_{0,1,2}) + O(^1D_2)$ are observed. By integrating the areas of the peaks, the three branching ratios listed above for the three CO predissociative states were obtained and listed in Table II. We note that the $C(^1D_2) + O(^3P_J)$ product channel is also energetically allowed in the present photodissociation study of CO. However, since this channel is not probed, and thus can be ignored in the analysis. By combining the fine-structure distribution determined for $C(^3P_{0,1,2})$ and the values for BR-I, BR-II, and BR-III given in Tables I and II, we can determine the branching ratios of the dissociation channels $C(^3P_0) + O(^1D_2)$: $C(^3P_1) + O(^1D_2)$: $C(^3P_2) + O(^1D_2)$: $C(^3P_0) + O(^3P_J)$: $C(^3P_1) + O(^3P_J)$: $C(^3P_2) + O(^3P_J)$ as (BR-I) × (F0): (BR-II) × (F1): (BR-III) × (F2): [1 − (BR-I)] × (F0): [1 − (BR-II)] × (F1): [1 − (BR-III)] × (F2). The branching ratios obtained using the above expressions are listed in Table III. For the two $^1\Sigma^+$ states $(4s\sigma)\ ^1\Sigma^+(v=4)$ and $(4p\sigma)\ ^1\Sigma^+(v=3)$ investigated, the C atoms in the $(^3P_0)$ state dominate the product formation accompanying with $O(^1D_2)$ with negligible amount of $C(^3P_2)$ and $C(^3P_1)$; while for the $^1\Pi$ state $[(4p\pi)\ ^1\Pi(v=3)]$, $C(^3P_1)$ dominates the process with much smaller relative amounts of $C(^3P_2)$ and $C(^3P_0)$.

The fine-structure distribution and correlated fine-structure branching ratio data provide the most detailed nonadiabatic interaction information in the dissociation process, starting from the intersystem crossing in the Franck-Condon region to the dissociation limits in the asymptotic region. A beautiful example is the study of the fine-structure distribution of the $O(^3P_{2,1,0})$ product in the predissociation of OH radical via the $A^2\Sigma^+$ state.[12,13] The near perfect agreement achieved between the theoretical calculations[12] and experimental measurements[13] has provided detailed understanding of the dissociation dynamics for this system. To quantitatively explain the current results of CO predissociation, detailed potential energy curves in this energy region are needed, including how many repulsive states are interacting with the directly excited states, and the strength of spin-orbit couplings between these states. All this information is currently unknown, making quantitative understanding of the predissociation dynamics of CO unfeasible at the present time. Based on the two totally different correlated spin-orbit branching ratios observed as given in Table III, there should be at least two different dissociative states that are, respectively, correlating to $C(^3P_0) + O(^1D)$ and $C(^3P_1) + O(^1D)$ in the asymptotic region. Nonadiabatic interactions usually exist between different dissociative states, and quantum interference effect can play important roles among the dissociation processes along different repulsive states in the asymptotic region.[12,13] To fully understand the correlated spin-orbit branching ratios determined in the present study, an exact full quantum *ab initio* calculation may be required.

W.M.J. was supported by National Science Foundation (NSF) under Grant No. CHE-0957872. C.Y.N. was supported by the Chemical Sciences, Geosciences and Biosciences Division, Office of Basic Energy Sciences, Office of Science, (U.S.) Department of Energy (DOE) under Contract No. DE-FG02-02ER15306.

[1]H. Kato and M. Baba, Chem. Rev. **95**(7), 2311 (1995).
[2]Y. Pan, H. Gao, L. Yang, J. Zhou, C. Y. Ng, and W. M. Jackson, J. Chem. Phys. **135**(7), 071101 (2011).
[3]H. Gao, L. Yang, Y. Pan, J. Zhou, C. Y. Ng, and W. M. Jackson, J. Chem. Phys. **135**(13), 134319 (2011).
[4]H. Gao, Y. Song, L. Yang, X. Shi, Q. Yin, C. Y. Ng, and W. M. Jackson, J. Chem. Phys. **135**(22), 221101 (2011).
[5]H. Gao, Y. Pan, L. Yang, J. Zhou, C. Y. Ng, and W. M. Jackson, J. Chem. Phys. **136**(13), 134302 (2012).
[6]H. Gao, Y. Song, L. Yang, X. Shi, Q.-Z. Yin, C. Y. Ng, and W. M. Jackson, J. Chem. Phys. **137**, 034305 (2012).
[7]Y. Song, H. Gao, C. Y. Ng, and W. M. Jackson, presented at the European Conference on Laboratory Astrophysics, Paris, 2011.
[8]A. H. Kung and Y. T. Lee, in *Vacuum Ultraviolet Photoionization and Photodissociation of Molecules and Clusters*, edited by C. Y. Ng (World Scientific, Singapore, 1991), p. 487.
[9]J. R. Lyons and E. D. Young, Nature (London) **435**, 317 (2005).
[10]M. Eidelsberg, F. Launay, K. Ito, T. Matsui, P. C. Hinnen, E. Reinhold, W. Ubachs, and K. P. Huber, J. Chem. Phys. **121**(1), 292 (2004).
[11]C. F. Fischer, J. Phys. B **39**(9), 2159 (2006).
[12]G. Parlant and D. R. Yarkony, J. Chem. Phys. **110**(1), 363 (1999).
[13]W. Zhou, Y. Yuan, and J. Zhang, J. Chem. Phys. **119**(19), 9989 (2003).
[14]D. J. Leahy, D. L. Osborn, D. R. Cyr, and D. M. Neumark, J. Chem. Phys. **103**(7), 2495 (1995).
[15]H. Kim, K. S. Dooley, G. C. Groenenboom, and S. W. North, Phys. Chem. Chem. Phys. **8**(25), 2964 (2006).
[16]K. S. Dooley, M. P. Grubb, J. Geidosch, M. A. van Beek, G. C. Groenenboom, and S. W. North, Phys. Chem. Chem. Phys. **11**(23), 4770 (2009).